Separation and Purification Technology 353 (2025) 128459

Contents lists available at ScienceDirect

Separation and Purification Technology

journal homepage: www.elsevier.com/locate/seppur

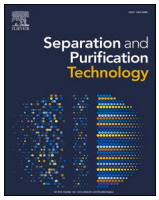

Enhancing fine particle removal by electrostatic precipitation from flue gas with a high PM concentration: Effect of various electrode configurations

Yifan Wang [a,b], Meng Yang [a], Lingyu Shao [a], Zhicheng Wu [a], Wenju Liu [d], Yaoji Chen [d], Chenghang Zheng [a,b,c,*], Xiang Gao [a,b,c]

[a] State Key Laboratory of Clean Energy Utilization, State Environmental Protection Engineering Center for Coal-Fired Air Pollution Control, Zhejiang University, Hangzhou 310027, People's Republic of China
[b] Institute of Carbon Neutrality, Zhejiang University, Hangzhou 310027, People's Republic of China
[c] Zhejiang Baima Lake Laboratory Co., Ltd., Hangzhou 310051, People's Republic of China
[d] Zhejiang Tiandi Environmental Protection Technology Co., Ltd., Hangzhou 311121, People's Republic of China

ARTICLE INFO

Editor: Luo Guangsheng

Keywords:
Electrostatic precipitator
Fine particle
Collection efficiency
Ionic wind
PIV

ABSTRACT

Particle pollution has hazardous effects on air quality and human health, especially fine particle. However, the highly efficient removal of fine particles is an unsolved problem in electrostatic precipitators (ESPs). In this study, a transparent ESP was designed to investigate the effect of fine particles on the corona discharge performance and the role of ionic wind in particle migration. And five types of typical discharge electrodes were applied. The results showed that the presence of fine particles could weaken the corona current produced by electrode discharge. Among these electrodes, the spike electrode can reduce the adverse effect of the particle space charge. The maximum ionic wind velocity around the electrode tips and within the near-plate region could reached 5.67 m/s and 5.00 m/s under an applied voltage of 30 kV, respectively. Combining the effects of corona discharge and ionic wind, the collection efficiencies of fine particles decreased in the following order: spike electrode (medium needle) > spike electrode (longest needle) > arista electrode > spike electrode (shortest needle) > sawtooth electrode. In general, spike electrode discharge has better performance for particle charging and particle collection efficiency and is suitable for fine particle removal in ESPs. In addition, electrode configuration/arrangement optimization methods were proposed to enhance fine particle removal in ESPs.

1. Introduction

PM pollution has attracted widespread attention in recent decades due to its hazardous effects on air quality and human health [1–3]. Electrostatic precipitators (ESPs) are an effective means of controlling particle emissions in coal-fired power plants [4], steel sintering [5] and other industries [6]. However, ESPs have relatively low collection efficiency for 0.1–1.0 μm particles [7–9]. The presence of fine particles could severely reduce the corona current and particle collection efficiency [10,11], even at low mass concentrations [12]. Moreover, fine particles can enter human lungs through breathing, thus damaging the respiratory system and even the cardiovascular system [13–15]. Therefore, increasing attention is paid on the fine particle removal characteristics through ESPs [16].

Corona discharge is the fundamental process for ESPs and is closely related to the removal efficiency [17–19]. To enhance the removal of particles, corona discharge processes with various electrode configurations have been studied in recent decades [20,21]. Jędrusik et al. [22,23] investigated the current–voltage characteristics and the discharge current distribution with diffident discharge electrodes to enhance the particles removal. The results showed that the design of configuration electrodes had a strong influence on particles removal performance of ESPs [24]. Rezinkina et al. [25] indicated that the discharge characteristics and electric field distribution in ESPs with different electrode configurations were closely related to the radius of curvature of the discharge electrode tips and the length of the needles. Andrade et al. [26] summarized the effects of the discharge electrode parameters such as number, diameter and spacing on the electric characteristics and the nanoparticle collection efficiency of a wire-plate ESP. Wang et al. [27] reported that increasing the symmetry of the electrode

* Corresponding author at: State Key Lab of Clean Energy Utilization, Institute for Thermal Power Engineering, Zhejiang University, Hangzhou 310027, People's Republic of China.
E-mail addresses: yfw1@zju.edu.cn (Y. Wang), zhengch2003@zju.edu.cn (C. Zheng).

https://doi.org/10.1016/j.seppur.2024.128459
Received 3 April 2024; Received in revised form 25 May 2024; Accepted 14 June 2024
Available online 21 June 2024

needle tip arrangement can increase the uniformity of the current distribution, which contributes to increasing the efficiency of the particle. However, the presence of fine particles would significantly affect the discharge characteristics of ESPs, which was called corona quenching or corona suppression [28,29]. This phenomenon was first discussed by Deutsch et al. [30] and further investigated by Sproull et al. [31], Elmoursi et al. [32], Awad et al. [33], and others. Our previous work also found that the current of a 660 MW coal-fired power plant decreased from 2170 mA to 100 mA when high concentration fine-particles was introduced, and the breakdown frequency increased by more than 2 times [34]. Unfortunately, the effect of fine particle on corona discharge and electrostatic precipitator is usually neglected in numerous investigations, and remain unclear.

Meanwhile, the ionic wind generated by corona discharge also influences electrostatic precipitation. Particle image velocimetry (PIV) is a typical method for investigating the flow field distribution [35,36]. Podlinski et al. [37–39] systemically studied the flow velocity distribution of the spike-plate type ESPs by PIV methods and concluded that change of the electrohydrodynamic secondary flow influenced ESP collection efficiency. Krupa et al. [40] investigated the velocity field of ionic wind flow with a needle discharge electrode by PIV measurements and found that back corona discharge can reduce the collection efficiency of particles in ESPs. Moreau et al. [41] concluded that the ionic wind generated by negative corona discharge was more stable. Moreover, various numerical models have been used to study the role of ionic wind in the flow field distribution and particle collection. Li et al. [42] considered the influence of temperature on the ionic wind and particle migration in the model, and found that the increase in temperature would aggravate the disturbance of ionic wind on the flow field. Shangguan et al. [43] established a corrugated plate ESP model to investigate the ionic wind evolution, and expecting to eliminate ionic wind vortex. Nevertheless, the influence of ionic wind on particle migration with various electrode configurations has not been investigated systematically, especially when high concentration fine-particles contained.

In recent years, various methods have been conducted to improve fine-particle removal performance in electrostatic fields, such as electrode configuration optimization [44], development of pulse power supply [45]. In addition, the removal efficiency of fine particles could also be improved by enlarging particle size, such as electrical agglomeration [46–48], chemical agglomeration [49], acoustic agglomeration [50]. Among them, electrode configuration optimization is an effective and recommended method [51–53]. Tong et al. [54] studied the corona discharge and collection efficiency of a honeycomb tube ESP equipped with arista electrodes and reported that improving the uniformity of the electric field strength can enhance particle removal. Niewulis et al. [55] found that the position of the discharge electrode could affect particle removal by measuring the collection efficiency of narrow ESPs with a longitudinal wire electrode. Arif et al. [56] studied the corona discharge characteristics of round rod electrodes and sawtooth electrodes and reported that sawtooth electrodes can significantly enhance the space ion density field, thereby improving the particle collection efficiency. However, fine particle removal in ESPs is a complex process, and interactions among corona discharge, gas flow and particle migration are still not clearly understood. Thus, having fundamental knowledge about corona discharge and ionic wind performance under flue gas with a high PM concentration is crucial in the promotion of ESP development with increasingly expectation of high-efficiency fine particle removal.

In this study, a transparent ESP was designed to investigate the effect of fine particles on the corona discharge performance and the role of ionic wind in particle migration, under simulated flue gas with a high PM concentration. Moreover, the maximum particle charge and particle collection efficiency of fine particles were systematically discussed to determine the effect of electrode configuration optimization on enhancing fine particle removal. The results provide a valuable reference for the effective removal of fine particles in ESPs.

2. Experimental setup and methods

2.1. Experimental system

A schematic of the experimental system is illustrated in Fig. 1. The system mainly consisted of a transparent ESP, a high-voltage power supply, particle image velocimetry (PIV) measurements, and an electrostatic low-pressure particle impactor (ELPI$^+$).

The transparent ESP mainly consisted of a discharge electrode, collection plate and flow channel. The schematic diagram of the flow channel was shown in Fig. 2(a), which was made of PTFE and silica glass (Hengyang Optical Technology, China). The internal flow channel was 600 mm in length, 150 mm in width and 100 mm in height. The residence time of the flue gas in the electric field was 0.2–2.0 s (gas flow was 1–0.1 m/s). Both the discharge electrode and collection plate were made from 316L stainless steel. The width and length of the collection plate were 150 mm and 200 mm, respectively. The symmetry axis of the discharge electrode was parallel to the collection plate, and placed in the center of the length and height of the flow channel. Five types of discharge electrodes used in this study is shown in Fig. 2(b) − (f). Among them, the tip cone angle of the spike electrodes was 30 °and the radius of the top tip was about 25 μm. The high-voltage power supply (SL60N600, Spellman, USA) had a maximum output voltage of 60 kV for corona discharge. A high-voltage resistor (R_2 = 5 MΩ) was connected to the system to prevent high-voltage breakdown. In addition, the corona current was converted by measuring the voltage across a constant value resistor (R_1 = 5 KΩ) with a voltage probe (TPP0500, Tektronix, USA). To ensure the accuracy of the experiment, the voltage outputted by high-voltage power supply was directly measured by a high-voltage probe (P150-G, Finechem, Japan).

The PIV measurements consisted of a high-speed camera (X150, Thousand Eyes Wolf, China) with a resolution of up to 2560 × 1920 pixels and a double-pulse Nd:YAG laser (SOLO PIV, New Wave, USA), which was used for the investigation of the flow field in the ESPs. The flow field was determined from two positions of the particles recorded with two consecutive laser pulses generated at 50 μs time intervals and with a 30 Hz repetition rate. The laser pulse energy was set as 120 mJ. For each measurement, instantaneous velocity fields were computed by an adaptive cross-correlation algorithm. From these instantaneous velocity fields, the time-averaged velocity field could be determined by the measuring system.

Due to its rapid response and high accuracy, ELPI$^+$ was appropriate for investigating the concentration and charges of particles with different diameters. Therefore, the charging characteristics of the particles were measured by an electrostatic low-pressure particle impinger (ELPI$^+$, Dekati, Finland), and connected with a vacuum pump (SV25B, Ernst Leybold, Ltd., Germany) in this study.

The simulated flue gas was provided by a fan with a maximum flow rate of 8.9 L/s. The fine particles of the simulated flue gas came from moxa-stick combustion. The mass concentration of the particles in the flue gas was maintained at 260.0 mg/m^3. The particle size distribution of the flue gas is presented in Fig. 3, and the median diameter of the particles was 0.29 μm.

2.2. Analytical methods

In this study, a voltage probe and a high-voltage probe were used to measure the voltage across the constant value resistor and the system, respectively. The voltage across the constant value resistor (R_1 = 5 kΩ) was measured as U_1 by the voltage probe, and the corona current generated between discharge electrode and collection plate was expressed as:

$$I = U_1/R_1 \tag{1}$$

The voltage between the discharge electrode and collection plate was calculated through U_2 measured by the high-voltage probe (the high-

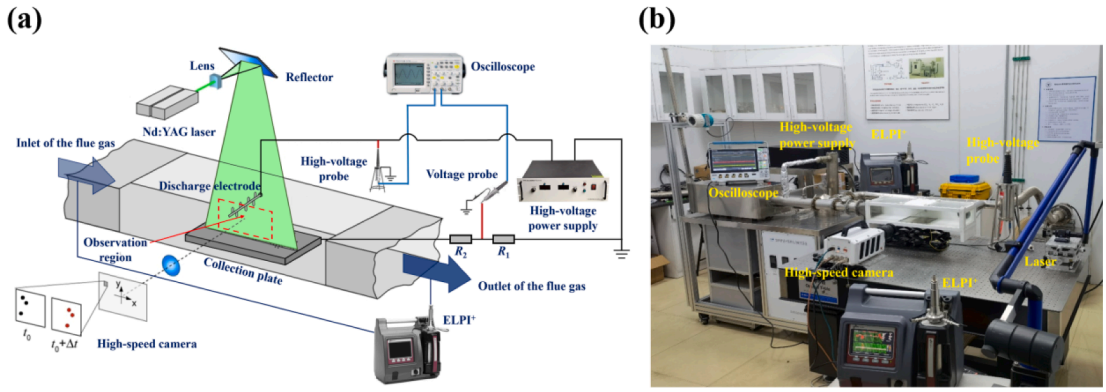

Fig. 1. Schematic of the experimental system: (a) schematic and (b) photograph.

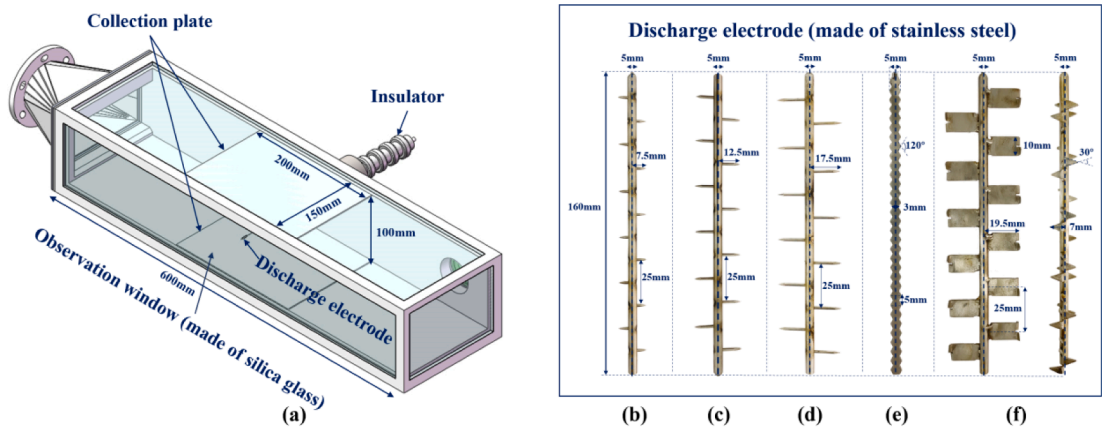

Fig. 2. Schematic diagram of (a) the flow channel and (b) – (f) discharge electrodes.

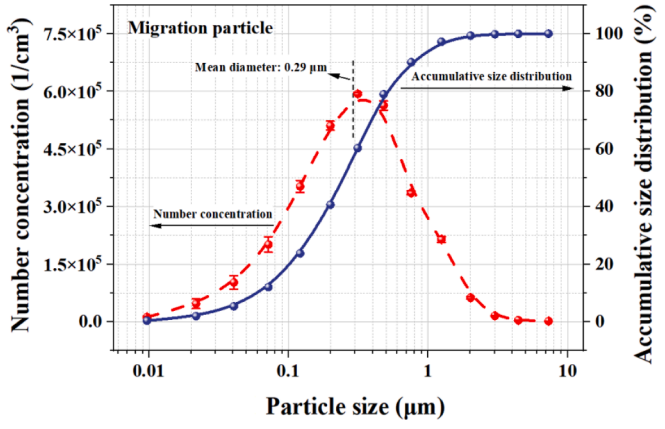

Fig. 3. Particle size distribution of the flue gas.

voltage probe divider ratio was 3000:1). The actual applied voltage of the ESP is shown as follows:

$$U = U_2 - (R_1 + R_2) \times I = U_2 - U_1 \times (R_1 + R_2)/R_1 \tag{2}$$

where R_2 is the protection resistor, $R_2 = 5M\Omega$.

The charging characteristics, number concentration, and mass concentration of the particles were measured by ELPI$^+$. During particle charge measurements, the relationship between the particle charge (q_p) and the fractional current is shown as follows:

$$q_p = I^* \Big/ \eta^* Q N_{outlet(i)} \tag{3}$$

where I^* is the fractional current measured by ELPI$^+$,η^* is the charging efficiency of the particles in ELPI$^+$, which is 100 % in this study [57], and Q is the sampling volume flow rate of ELPI$^+$ (10 L/min), $N_{outlet(i)}$ is fractional particle number concentrations (cm^{-3}) at the channel outlet with corona discharge.

The performance for particle collection in ESPs was evaluated by the collection efficiency (η) calculated using the following equation:

$$\eta = \left(\sum_{i=1}^{n} c_{inlet(i)} - \sum_{i=1}^{n} c_{outlet(i)} \right) \Big/ \sum_{i=1}^{n} c_{inlet(i)} \times 100\% \tag{4}$$

where $c_{inlet(i)}$ and $c_{outlet(i)}$ are the fractional particle mass concentrations (mg/cm^3) at the channel outlet without and with corona discharge, respectively.

The index of specific energy density (*SED*) was defined to reflect energy input and economic benefit during corona discharge with various electrode configuration [58]:

$$SED = (UI)/Q_{ESP} \tag{5}$$

where U is the applied voltage (kV), I is the corona current (mA), and Q_{ESP} is the gas flow rate (m^3/s).

The error bar is determined by standard error (*SE*), which is the quotient of the standard deviation (*SD*) and the square root of the sample numbers.

$$SE = SD \Big/ \sqrt{N} \tag{6}$$

$$SD = \sqrt{\frac{\sum (X_i - \overline{X})^2}{(N-1)}} \quad (7)$$

where $\overline{X}$ is the mean of the samples, and X_i is the value of the i-th sample; N is the number of repetitive experiments.

3. Results and discussion

3.1. Effect of fine particles on the corona discharge performance

In practical applications, the presence of particles can contribute to the complexity of coupled processes in ESPs. Particles can collide with ions to form the particle space charge, which resulting in a weakening of the corona discharge performance. This effect could be more obvious for fine particles even at much lower mass concentrations, and cannot be neglected in electrostatic precipitation.

Fig. 4(a) shows the effect of the needle length on the V-I characteristic with and without fine particles. Under air conditions, the breakdown voltage decreased with the length of the needle. The maximum corona currents of spike electrodes with various needle lengths were in the following sequence: shortest needle > medium needle > longest needle. With the injection of the high concentration fine-particles, both the corona current and breakdown voltage were decreased. The adverse effect of the particle space charge decreased with the length of the needles, with the maximum corona current decreasing by only 17.1 % for the longest needle and by 50.8 % for the shortest electrode. However, the increase in electrode needle length also reduced the breakdown voltage during the electrostatic precipitation process. Under the combined effects, the medium needle had the best performance for corona discharge when treating flue gas with high concentration fine particles.

The corona discharge performances of the sawtooth electrode and the arista electrode are shown in Fig. 4(b). The arista electrode was also strongly affected by the effect of the particle space charge, and the maximum corona current decreased by more than 30 %. The sawtooth electrode was almost unaffected by the effect of the particle space charge, which can be attributed to the presence of more electrode tips, which dispersed the influence of the particle space charge. However, the corona current of the sawtooth electrode were both low under air and fine particle injection conditions, which was not favorable for particle removal. Ultimately, the maximum corona current of the various electrodes in the presence of fine particles decreased in the following sequence: spike electrode (medium needle) > spike electrode (shortest needle) > arista electrode > spike electrode (longest needle) > sawtooth electrode. The above experimental results showed that the spike electrode can reduce the adverse effect of the particle space charge, which is beneficial for the removal of fine particles. In practical applications, if the flue gas contains high concentration fine-particles, it is recommended to use a spike electrode. And appropriate increasing in needle length and number was suggested.

The presence of fine particles also influenced the corona onset voltage of the ESP. The variations in the corona onset voltage of the five discharge electrodes under air and fine particle injection conditions were studied comparatively, as shown in Fig. 5. The corona onset voltage of the spike electrode was significantly lower than that of the arista electrode and the sawtooth electrode. In addition, the corona onset voltage of the spike electrode decreased with the needle length. With the injection of flue gas, electrons released from needle tips were trapped by the fine particles, which led to an increase in the corona onset voltage. However, for the arista electrode and sawtooth electrode, the injection of fine particles decreased the corona onset voltage. The phenomenon could be attributed to the higher corona-onset voltage of the arista electrode and sawtooth electrode. In this moment, particle polarization made higher electric field strength near the discharge electrode. When the electric force exceeds the surface tension of the particles, particles breakage will occur, which may promote the occurrence of corona discharge [59]. This phenomenon may also be affected

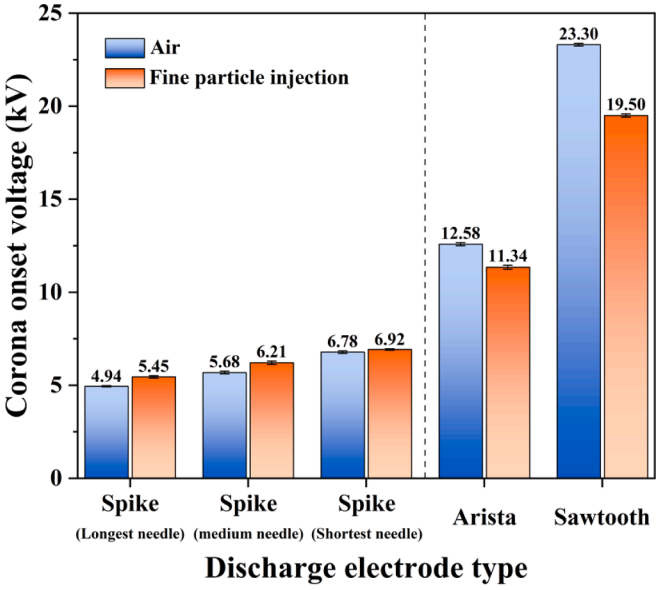

Fig. 5. Effect of the fine particle injection on the corona onset voltage.

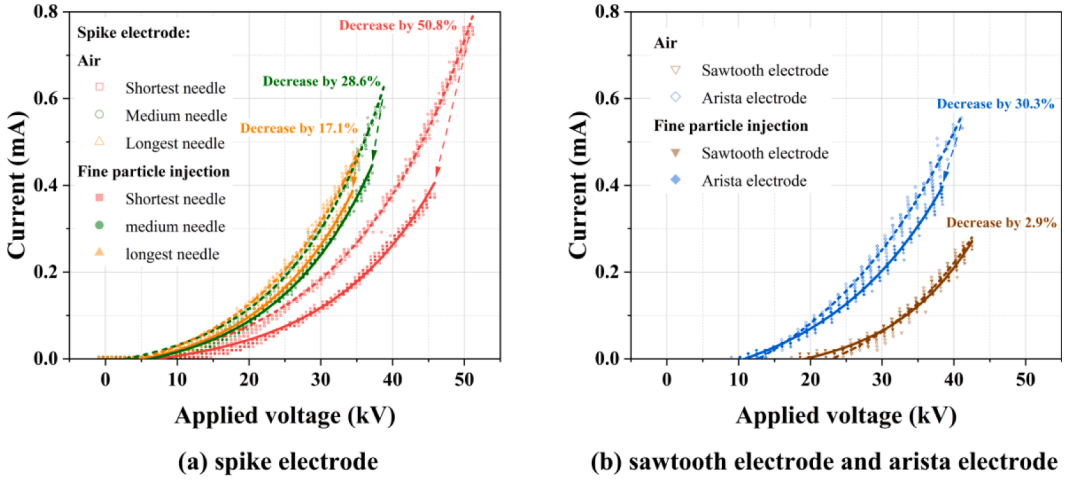

Fig. 4. Effect of discharge electrode on corona discharge characteristics.

by particle size, particle dielectric constant, particle concentration, etc. As a result, the corona onset voltage of the sawtooth electrode decreased from 23.30 kV to 19.50 kV when fine particles were injected. And the corona onset voltage of the arista electrode only decreased 1.24 kV.

The effect of the electrode arrangement on the corona discharge characteristics is illustrated in Fig. 6. When the electrode tip was arranged vertical to the collection plate, it exhibited a higher corona discharge and electric field strength. This mainly arose from the shorter interelectrode distance in the vertical arrangement, which reduced losses during ion migration. Moreover, it was found that the vertical spike electrode was better at weakening the adverse effect of the particle space charge. The maximum corona current for vertical spike electrode decreased by 17.1 %, whereas the corona current reduction for the horizontal spike electrode reached 45.9 %. Consequently, in practical applications, arranging the discharge electrode tips vertically to the collection plate was recommended to enhance the corona current, particularly for the flue gas containing high concentration fine particles.

3.2. Insight into the role of ionic wind in particle migration

The effect of fine particles on the corona discharge performance is analyzed in the above sections, while the ionic wind generated by corona discharge also influences electrostatic precipitation. Ionic wind is created by the electrohydrodynamic propulsive force in electrically charged fluids, which consists of ionized and neutral air molecules. High-speed ionic wind can disturb the flow field distribution, which also influences the migration and collection of charged particles. Therefore, it is also essential to further investigate the effect of ionic wind on particle migration. The initial flow rate at the inlet was set as 0.1 m/s.

3.2.1. Effect of applied voltages

Fig. 7 illustrates the ionic wind distribution under different applied voltages, and spike electrode (longest needle) was selected as discharge electrode. It was obvious that under a low applied voltage (10 kV), the ionic wind produced a slight disturbance to the inlet flue gas and generated a large-scale vortex in the region upstream of the electrode. With the increasing in applied voltage, the disturbance effect of the ionic wind was more obvious, and the area of the influence region gradually broadened. Notably, obvious vortices were observed in both the upstream and downstream regions of the electrode in this moment.

3.2.2. Effect of discharge electrodes

The difference in corona discharge characteristics among various discharge electrodes inevitably results in the change of ionic wind distributions, as shown in Fig. 8. To clearly illustrate the variations in the ionic wind distribution generated by the corona discharge of different electrodes, and the applied voltage was maintained at 30 kV. As shown in Fig. 8a-c, high-speed ionic wind drove the flue gas spread on both sides of the discharge electrode, which became increasingly obvious as the needle length of discharge electrode. When the needle length reached 10 mm (medium needle), a clear vortex appeared in the upstream region of the discharge electrode. With the needle length further increased to 15 mm (longest needle), the vortex further expanded and collided with the incoming flow. Although the ionic wind generated by one electrode tip of the sawtooth electrode was weak, the sawtooth electrode has numerous electrode tips, and the ionic wind produced by the nearby tips interacted with each other to form many vortices in ESP, as shown in Fig. 8d. The disturbance of the flue gas generated by the arista electrode differed from that of the above electrode types. There were two high-velocity regions of ionic wind, as displayed in Fig. 8e. The weaker ionic wind region in the upstream region was generated by nearby electrode tip, whereas the stronger ionic wind region in the downstream region originated from the indicated electrode tip. These two components of ionic wind both promote fine particle migration toward the collection plate.

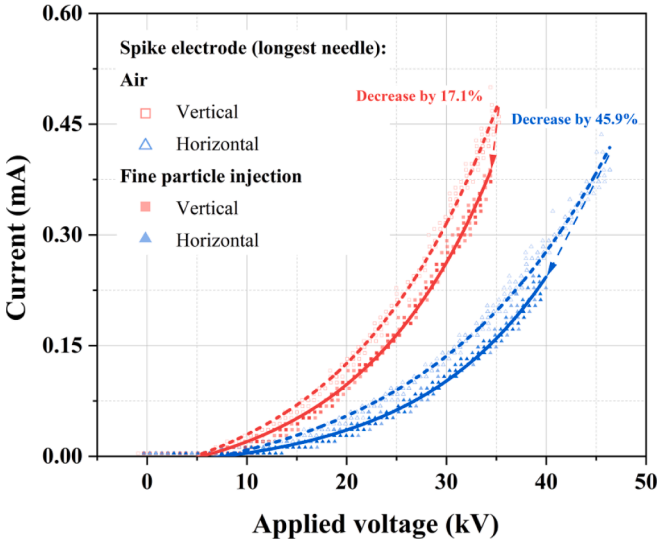

Fig. 6. Effect of electrode arrangement on corona discharge characteristics.

To further investigate the effect of ionic wind on particle migration, the flow field distributions around the needle tip and within the near-plate region were studied. The flow field distribution around the electrode tip was measured at 1 mm below the needle tip, and the flow field distribution within the near-plate region was measured at 1 mm above the collection plate. Fig. 9 displays the flow field distribution around the needle tip with different discharge electrodes. The velocity distribution near the tips of all discharge electrodes exhibited a 'V'-shape, with the highest velocity occurring near the electrode tips, which can drive the migration of surrounding particles. The maximum velocities of the ionic wind near the electrode tips were in the following sequence: spike electrode (longest needle) > spike electrode (medium needle) > arista electrode > spike electrode (shortest needle) > sawtooth electrode. The maximum ionic wind velocity of spike electrode could reach 5.67 m/s. Notably, the sawtooth electrode had the lowest intensity of corona discharge, but the velocity of the ionic wind could still reach 2.71 m/s.

Fig. 10 shows the flow field distribution within the near-plate region with different discharge electrodes. The ionic wind generated by spike electrode exhibited a stronger scouring effect on the collection plate. The ionic wind velocities of spike electrode with longest needle, medium needle, and shortest needle within the near-plate region could reach 5.00 m/s, 4.23 m/s, and 3.77 m/s, respectively. Additionally, the locations of the strongest ionic winds were closely related to the positions of the electrode tips. The flow field distribution of the arista electrode within the near-plate region displayed two obvious peaks, with the downstream region exhibiting higher velocities (up to 3.00 m/s). The sawtooth electrode induced relatively uniform disturbances within the near-plate region. Due to the influence of backflow, the upstream region had higher velocities (up to 2.39 m/s). The maximum velocity of the arista electrode was weaker than that of the shortest needle electrode within the near-plate region, which was reversed from the sequence of ionic wind distributions near the electrode tip. This was mainly attributed to the more concentrated ion beam produced by corona discharge of the spike electrode, resulting in less dissipation during its migration to the collection plate. Ultimately, the maximum ionic wind velocities within the near-plate region were in the following sequence: spike electrode (longest needle) > spike electrode (medium needle) > spike electrode (shortest needle) > arista electrode > sawtooth electrode.

3.2.3. Effect of electrode arrangement

Fig. 11 shows the ionic wind distribution of the spike electrode when the electrode tip was arranged horizontally. And there are two types of electrode tips horizontal arrangement, which was faced same or opposite direction to the inlet flue gas. The ionic wind of both arrangements

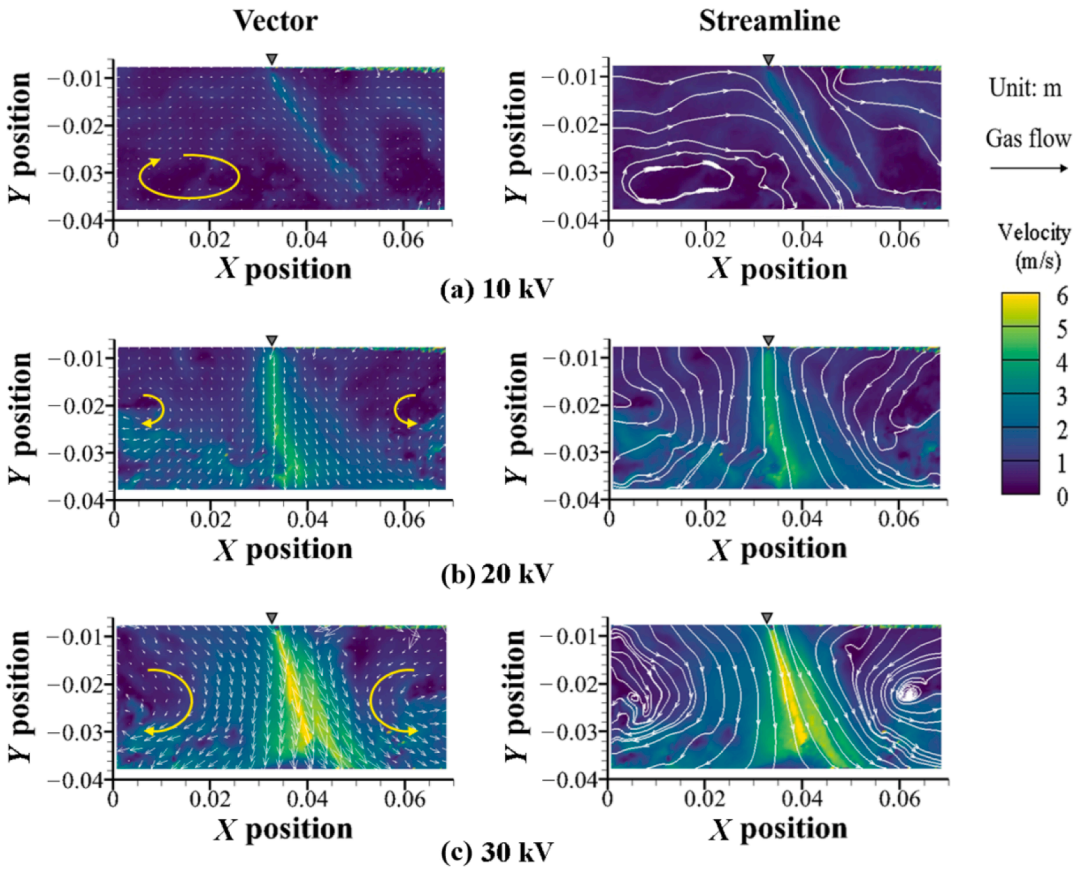

Fig. 7. Ionic wind distribution of the spike electrode under different applied voltages.

disturbed the inlet flue gas and created vortices, but the effect on particle migration was differential. When the electrode tips faced to the inlet flue gas, the ionic wind generated by the electrode promoted particles toward the collection plate, which is beneficial to particle removal. Conversely, when the electrode tips are in same direction to the inlet flue gas, the ionic wind can accelerate the movement of flue gas, further reducing the residence time of the particles in the electrostatic field, which is unfavorable for particle removal. Consequently, in practical applications, when electrode tips are arranged horizontal to the collection plates, the electrode tips should be installed facing to flue gas, which can promote particle migration through the transport of ionic wind.

A comparison of the flow field distribution around the electrode tip when the electrode was in a horizontal/vertical arrangement is shown in Fig. 12. Compared with the horizontal arrangement, the maximum velocity of ionic wind near the electrode tips in the vertical arrangement was obviously enhanced. However, the difference in the maximum velocity of the ionic wind between the two horizontal arrangement types (left or right) was not significant, with only a 0.02 m/s in difference. This indicated that the direction of inlet flue gas did not significantly impact the ionic wind formation.

Fig. 13 illustrates the influence of electrode tip arrangement on the flow field distribution within the near-plate region. Compared with the vertical arrangement, the scouring effect of the ionic wind on the collection plate surface was significantly weakened when the electrode tips were arranged horizontally. And obvious high-velocity regions of the ionic wind were not appeared in the electrode horizontal arrangement. Therefore, the horizontal arrangement of the electrode tip was suitable for the removal of large-size particles. For this electrode arrangement, a higher applied voltage could be reached, which introduces the higher particle charge and promotes the migration towards collection plates. Moreover, this electrode arrangement could weaken the scouring effect of ionic wind on deposited particles, which prevented particle re-entrainment.

3.3. *Enhancing fine particle removal by electrode configuration optimization*

The above discussion indicates that the presence of a high concentration fine-particles weakened the corona discharge process within ESPs, and ionic wind could also influence particle migration. In this section, particle charging and removal performance were investigated with different electrode configurations, and the initial flow rate at the inlet was set as 0.6 m/s. Moreover, some methods for enhancing fine particle removal by electrode configuration optimization were proposed.

Fig. 14 displays the effect of the electrode configuration on the maximum particle charge. Notably, the maximum particle charge was normalized, where the baseline (Q_{ref}) was the maximum particle charge of the spike electrode (shortest needle) with different particle sizes. Typically, there are two mechanisms within particle charging process (diffusion charging and field charging), which are closely related to the corona current and applied voltage, respectively. Under the combined action of two charging mechanisms, the maximum particle charge of various sizes decreased in the following sequence: spike electrode (medium needle) > spike electrode (longest needle, vertical arrangement) > arista electrode > spike electrode (shortest needle) > spike electrode (longest needle, horizontal arrangement) > sawtooth electrode. Moreover, with the increasing in particle size, the role of electrode configuration optimization in particle charge enhancement was gradually weakened. In terms of spike electrode, when the shortest needle was replaced by the medium needle electrode, the maximum charge of 9.67 nm particles was increased by 1.79 times. With the particle size increased to 199.59 nm, this increase in the maximum particle charge

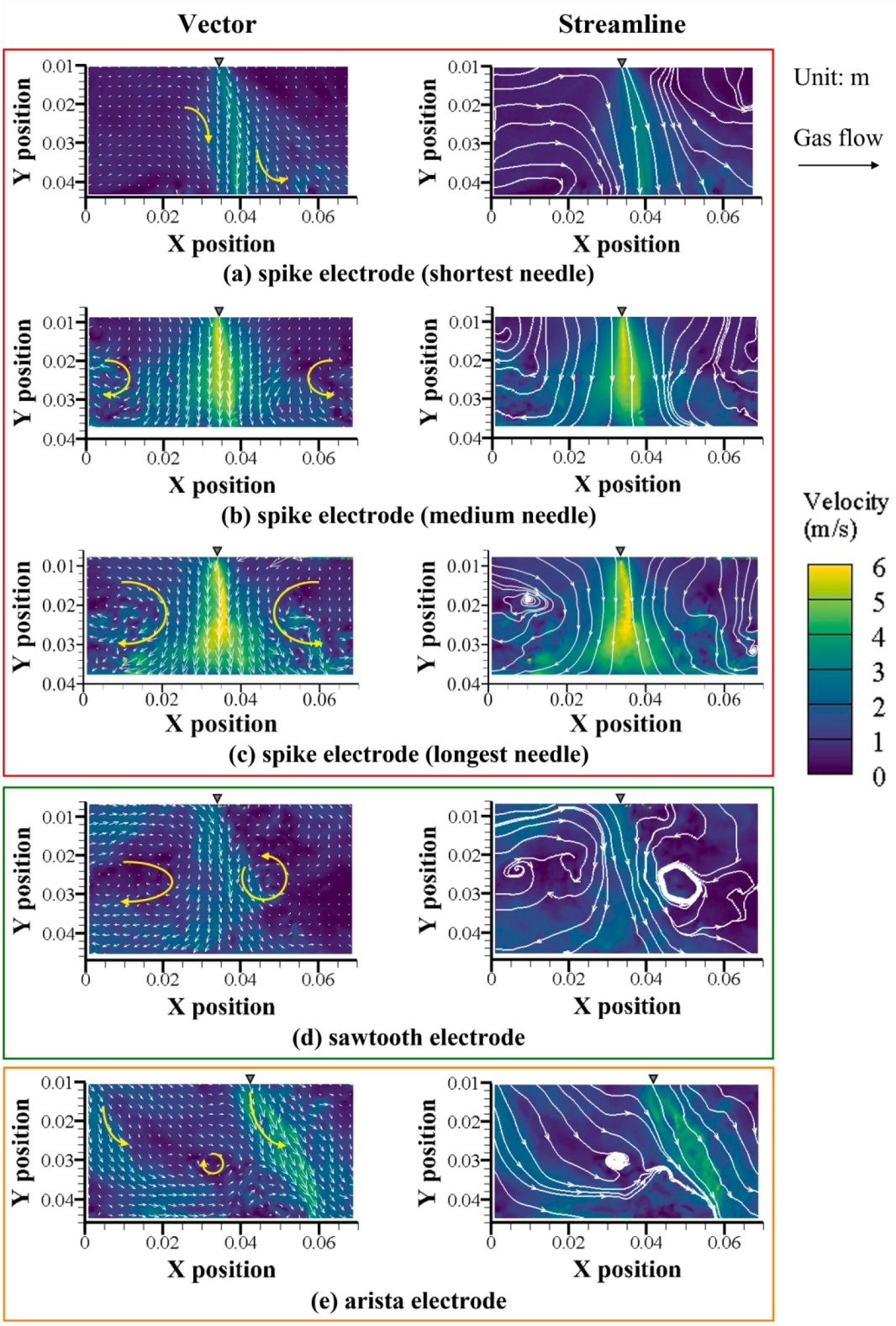

Fig. 8. Ionic wind distribution with different discharge electrodes.

was only 0.66 times. Moreover, the horizontal arrangement of the electrode tips was not beneficial for the particle charging process, especially for fine particles.

Fig. 15(a) shows the particle collection efficiency of various discharge electrodes under different applied voltages. The particle collection efficiencies of the spike electrode with longest needle or medium needle, and sawtooth electrode all increased with applied voltage. However, the particle collection efficiency of the spike electrode with shortest needle and the arista electrode initially increased and then decreased with the increasing in applied voltage. This may be attributed to gas ionization occurring on the charged particle surface under high applied voltage, especially near the discharge electrode and

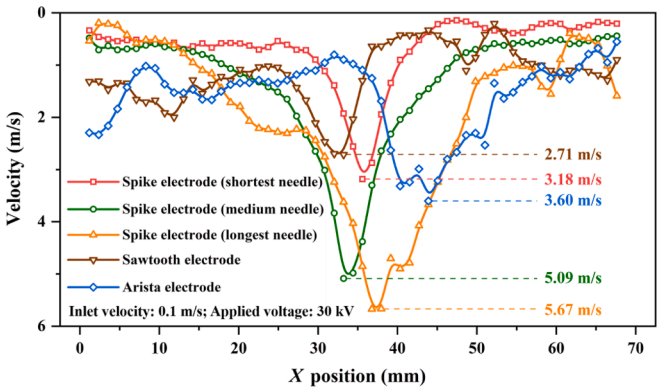

Fig. 9. Flow field distribution around the needle tip with different discharge electrodes.

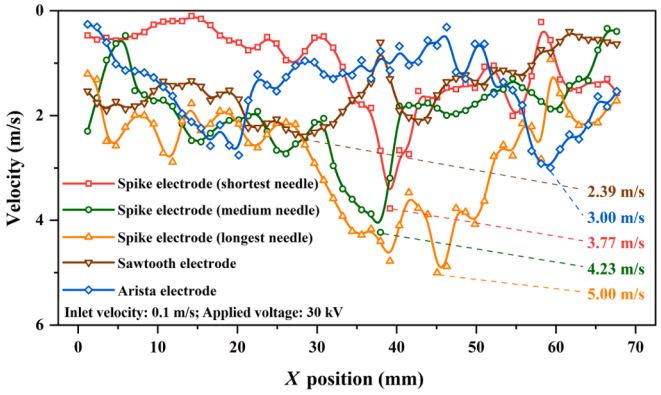

Fig. 10. Flow field distribution within the near-plate region with different discharge electrodes.

the collection plate. In this moment, high-voltage breakdown between the gap of particles was occurred. Meanwhile, the ionic wind was weak for this discharge electrode. Under the comprehensive effect of breakdown and ionic wind, the particle charge could not increase or even decreased with applied voltage, and result in the decreasing of collection efficiency.

Additionally, increasing the needle length could both increase the corona current and particle collection efficiency, but it also decreased the maximum applied voltage. The particle collection efficiency of the spike electrode with longest, medium and shortest needle electrodes were 76.2 %, 72.4 % and 60.2 % at an applied voltage of 30 kV, respectively. In this applied voltage, the spike electrode with longest needle had a better particle removal performance. With the applied voltage further increased, the spike electrode with longest needle quickly reached breakdown voltage and failed to stable operation. However, the spike electrode with medium needle or shortest needle electrodes could still discharge normally, and the particle collection efficiencies continued to increase with applied voltage. Ultimately, the particle collection efficiency of the spike electrode with medium needle could reach 82.3 %. Although the spike electrode with shortest needle could apply higher voltages without breakdown, the maximum collection efficiency was only 64.4 % due to the weak discharge strength.

In conclusion, the maximum particle collection efficiencies of the various discharge electrodes were in the following sequence: spike electrode with medium needle (82.3 %) > spike electrode with longest needle (76.2 %) > arista electrode (70.6 %) > spike electrode with shortest needle (64.4 %) > sawtooth electrode (33.1 %), which is in consistent order with the maximum particle charge with different electrodes. In practical applications, ESPs often applied highest voltage to ensure excellent particle collection performance. Therefore, it was crucial to consider both the particle removal efficiency at same voltage and the breakdown voltage when selecting the discharge electrode. For the fine particle removal, the spike electrode was more suitable than the arista electrode and sawtooth electrode due to combined effect of the higher corona-discharge intensity and the stronger ionic wind. And the needle length of discharge electrodes should be chosen within an appropriate range, rather than aiming excessively for a high corona discharge intensity.

Fig. 15(b) illustrates particle collection efficiency under different specific energy densities with various discharge electrodes. As the specific energy density increased, the collection efficiency of all discharge electrodes increased continuously. Among them, the increase in specific energy density had a relatively weak influence on particle collection efficiency of sawtooth electrodes. For example, the collection efficiency of spike electrode with medium needle increased from 23.7 % to 82.3 % when the specific energy density increased from 18.8 to 2593.3 J/m^3. But the collection efficiency of sawtooth electrodes only increased from 13.2 % to 33.1 % when the specific energy density increased from 51.0 to 940.3 J/m^3. At the same collection efficiency, the required specific energy density of spike electrode with medium or longest needle was obviously smaller than that of the sawtooth electrode and the arista electrode, especially for spike electrode with longest needle. Therefore, the spike electrodes have better economic benefits and collection efficiencies when treating flue gas with a high fine particle concentration in practical application.

Due to the better particle removal performance of the spike electrode, the spike electrode with longest needle was chosen here to investigate the effect of electrode arrangement on the particle collection efficiency, as shown in Fig. 16(a). For the vertical arrangement of discharge electrode, it both showed excellent collection performance of fine particles under the same applied voltage and maximum applied voltage. Although the horizontal arrangement of discharge electrode could maintain stable corona discharge at higher applied voltage, the particle collection efficiency was only reach 54.2 %. Fig. 16(b) shows particle collection efficiencies of various electrode arrangement under different specific energy densities. It indicates that the vertical arrangement of discharge electrode can combine higher collection efficiency and less energy input. Hence, for fine particle removal, it was advisable to arrange the discharge electrode vertical to the collection plate to enhance corona discharge and improve the particle collection efficiency.

4. Conclusion

In this study, a transparent ESP was designed to investigate the effect of fine particles on the corona discharge performance and the role of ionic wind in particle migration. Moreover, some methods for enhancing fine particle removal by electrode configuration optimization were proposed. The main conclusions are as follows:

(1) The presence of fine particles can weaken the corona current generated by electrode discharge. The maximum corona current of each electrode in the presence of fine particles followed the sequence: spike electrode (medium needle) > spike electrode (shortest needle) > arista electrode > spike electrode (longest needle) > sawtooth electrode. The spike electrode can reduce the adverse effect of the particle space charge, which is beneficial for the removal of fine particles. The corona onset voltage of the spike electrode was increased with fine particle injection, but it was decreased for the arista electrode and sawtooth electrode.

(2) The ionic wind generated by electrode discharge significantly disturbs the flow field distribution. The maximum ionic wind velocity of spike electrode could reach 5.67 m/s, and the ionic wind generated by sawtooth electrode could still reach 2.71 m/s. Meanwhile, the ionic wind exhibited a strong scouring effect on the collection plate. The ionic wind velocities of spike electrode

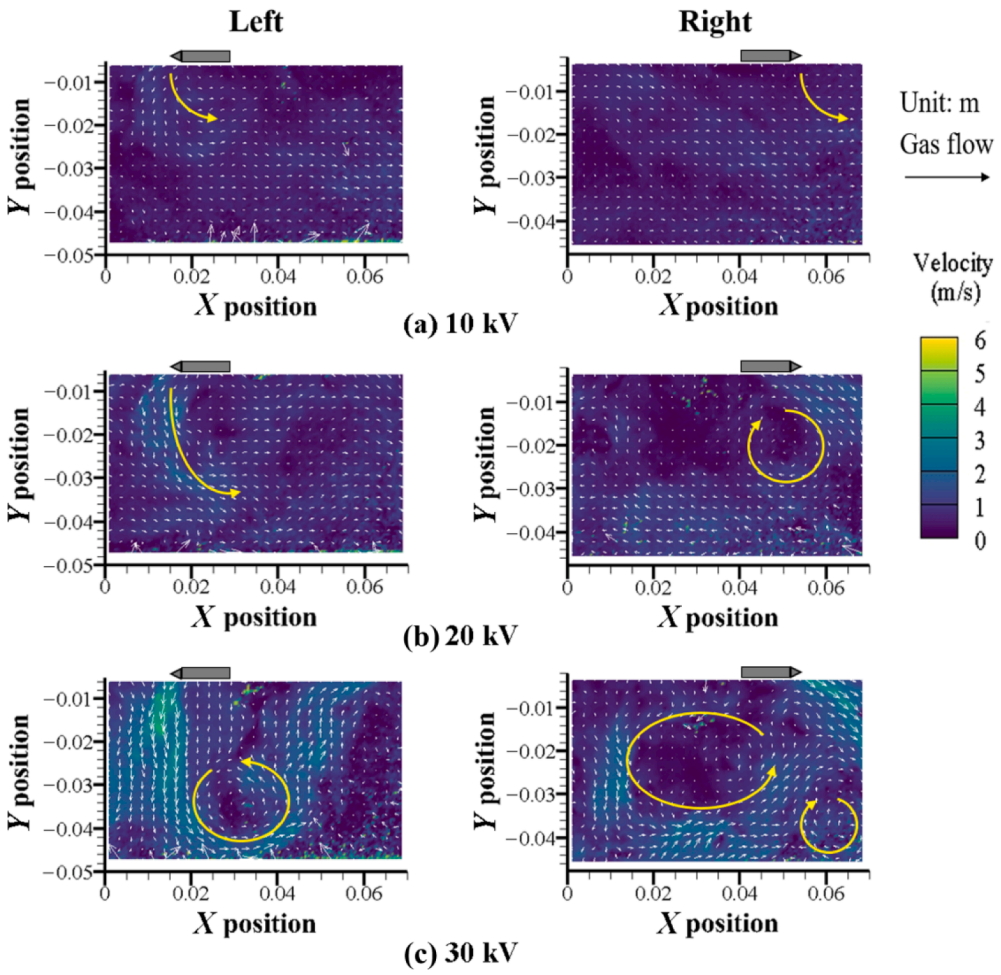

Fig. 11. Ionic wind distribution of the spike electrode when the electrode tip was arranged horizontally.

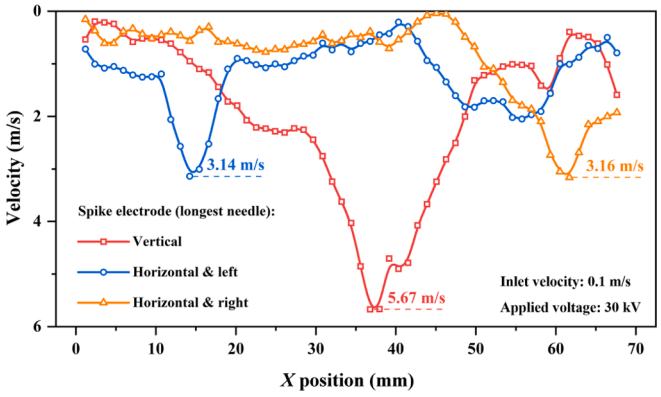

Fig. 12. Comparison of the flow field distribution around the electrode tip when the electrode was in a horizontal/vertical arrangement.

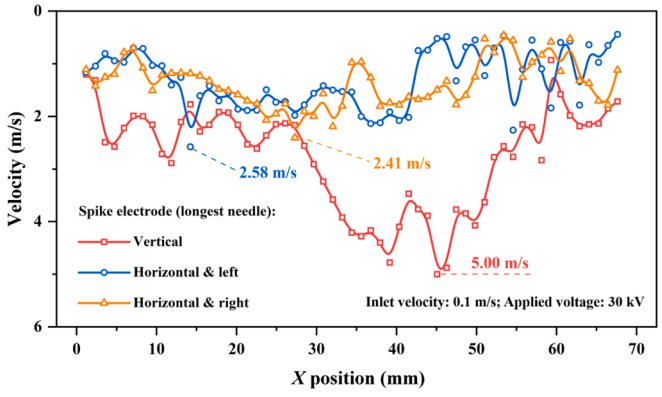

Fig. 13. Comparison of the flow field distribution within the near-plate region when the electrode is in a horizontal/vertical arrangement.

within the near-plate region could reach 5.00 m/s. Moreover, electrode horizontal arrangement could weaken the scouring effect of ionic wind on deposited particles, which prevented particle re-entrainment.

(3) The optimization of electrode configuration is an effective method for enhancing particle charging and improving particle collection efficiency. The maximum fine-particle collection efficiencies of the various discharge electrodes were in the following sequence: spike electrode with medium needle (82.3 %) > spike electrode with longest needle (76.2 %) > arista electrode (70.6 %) > spike electrode with shortest needle (64.4 %) > sawtooth electrode (33.1 %), which is in consistent order with the maximum particle charge with different electrodes. Spike electrode has excellent performance for particle removal in ESPs, and the number and length of needles could be appropriately increased when treating flue gas with a high PM concentration in practical application.

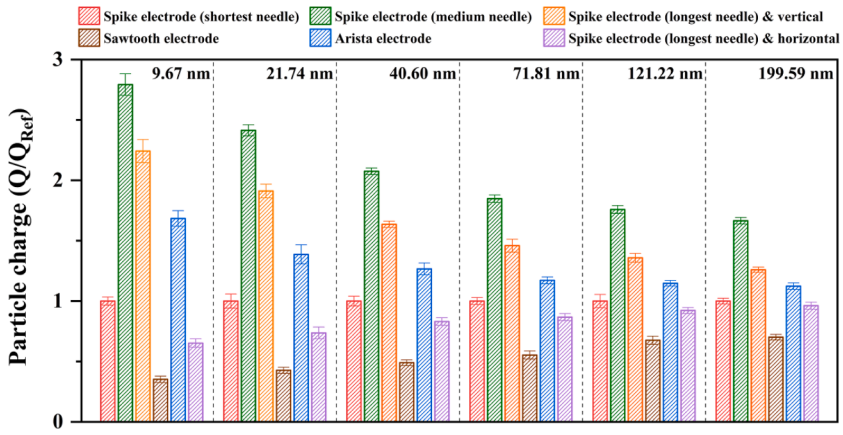

Fig. 14. Effect of electrode configuration on the maximum particle charge.

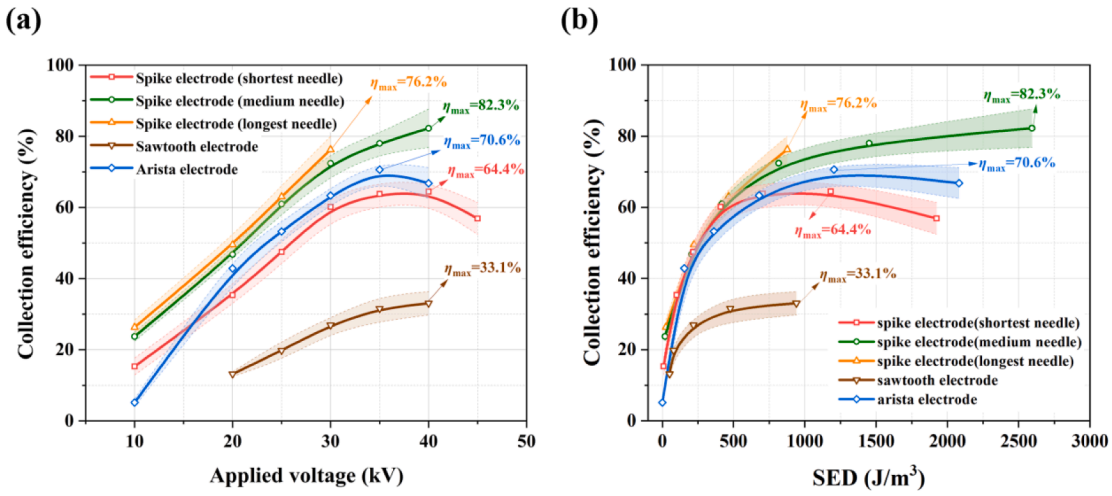

Fig. 15. Particle collection efficiency of various discharge electrodes under different (a) applied voltages and (b) specific energy densities.

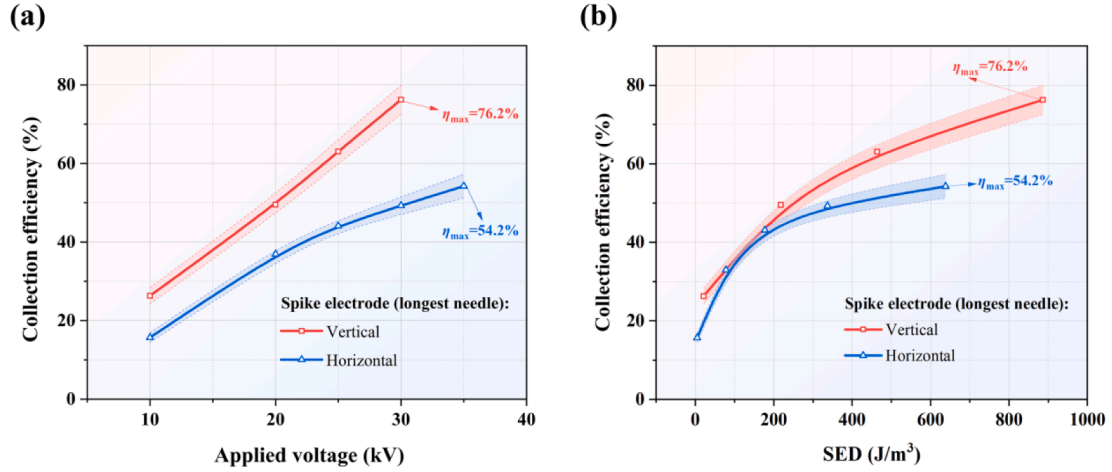

Fig. 16. Particle collection efficiencies of various electrode arrangement under different (a) applied voltage and (b) specific energy densities.

CRediT authorship contribution statement

Yifan Wang: Writing – review & editing, Writing – original draft, Methodology, Investigation, Conceptualization. **Meng Yang:** Writing – review & editing, Writing – original draft, Investigation, Data curation. **Lingyu Shao:** Writing – review & editing, Validation, Investigation. **Zhicheng Wu:** Writing – review & editing, Investigation, Data curation. **Wenju Liu:** Validation. **Yaoji Chen:** Validation. **Chenghang Zheng:** Supervision, Resources, Project administration. **Xiang Gao:** Supervision, Resources, Project administration.

Declaration of competing interest

The authors declare that they have no known competing financial interests or personal relationships that could have appeared to influence the work reported in this paper.

Data availability

Data will be made available on request.

Acknowledgments

This work was supported by the National Natural Science Foundation of China (52306279, 52076191, 42341208), the "Pioneer" and "Leading Goose" R&D Program of Zhejiang (2023C03008), and the Fundamental Research Funds for the Central Universities (2022ZJJH02-03).

References

[1] L. Henneman, C. Choirat, I. Dedoussi, F. Dominici, J. Roberts, C. Zigler, Mortality risk from United States coal electricity generation, Science 382 (2023) 941–946.
[2] T. Chen, L. Deng, Y. Li, J. Li, X. Zhao, L. Fu, Removal of multiple pollutants in air pollution control devices of a coal-fired boiler installed with a flue gas condensation scrubber, J. Clean. Prod. 434 (2024) 139971.
[3] M. Miao, T. Zhou, M. Zhang, R. Bai, H. Yang, Transformation of CFB boilers pollutant treatment strategies under China's stricter requirements and the background of carbon neutrality (FBC24), Fuel 342 (2023) 127009.
[4] Q. Tang, X. Zhao, L. Chen, H. Yao, C. Miao, Q. Ji, D. Ma, S. Zhang, Removal and emission characteristics of hazardous trace elements in total and graded particulate matters: a case study of a typical ultra-low emission coal-fired power plant, Sci. Total Environ. 908 (2024) 168434.
[5] H. Yi, T. Zhong, J. Liu, Q. Yu, S. Zhao, F. Gao, Y. Zhou, S. Wang, X. Tang, Emissions of air pollutants from sintering flue gas in the Beijing-Tianjin-Hebei area and proposed reduction measures, J. Clean. Prod. 304 (2021) 126958.
[6] R.B. Bist, X. Yang, S. Subedi, C.W. Ritz, W.K. Kim, L. Chai, Electrostatic particle ionization for suppressing air pollutants in cage-free layer facilities, Poult. Sci. 103 (2024) 103494.
[7] Y. Zhu, S. Tao, C. Chen, J. Liu, M. Chen, W. Shangguan, Highly effective removal of PM2.5 from combustion products: an application of integrated two-stage electrostatic precipitator, Chem. Eng. J. 424 (2021) 130569.
[8] Y. Song, Y. Zhang, Y. Liu, W. Long, K. Tao, K. Vafai, Numerical simulation of the collection efficiency of welding fume particles in electrostatic precipitator, Powder Technol. 415 (2023) 118173.
[9] J. Zhang, J. Wang, H. Ren, J. Fu, J. Li, Z. Zhang, Enhancement of $PM_{2.5}$ removal efficiency in high-temperature ESP under multi-field coupling: a numerical simulation study on temperature and magnetic field effects, Powder Technol. 434 (2024) 119376.
[10] A. Jaworek, A.T. Sobczyk, A. Krupa, A. Marchewicz, T. Czech, L. Śliwiński, Hybrid electrostatic filtration systems for fly ash particles emission control. A review, Sep. Purif. Technol. 213 (2019) 283–302.
[11] Y. Zhu, S. Tao, X. Yang, J. Liu, M. Chen, W. Shangguan, Improve removal efficiency of PM 1 depending on collision enhancement and agglomeration effect, Fuel Process. Technol. 252 (2023) 107981.
[12] Z. Yang, C. Zheng, S. Liu, Y. Guo, C. Liang, X. Zhang, Y. Zhang, X. Gao, Insights into the role of particle space charge effects in particle precipitation processes in electrostatic precipitator, Powder Technol. 339 (2018) 606–614.
[13] C. Zheng, Y. Wang, X. Zhang, Z. Yang, S. Liu, Y. Guo, Y. Zhang, Y. Wang, X. Gao, Current density distribution and optimization of the collection electrodes of a honeycomb wet electrostatic precipitator, RSC Adv. 8 (2018) 30701–30711.
[14] H. Yuk, S. Yang, S. Wi, Y. Kang, S. Kim, Verification of particle matter generation due to deterioration of building materials as the cause of indoor fine dust, J. Hazard. Mater. 416 (2021) 125920.
[15] M.M. Badami, R. Tohidi, M. Aldekheel, V.J. Farahani, V. Verma, C. Sioutas, Design, optimization, and evaluation of a wet electrostatic precipitator (ESP) for aerosol collection, Atmos. Environ. 308 (2023) 119858.
[16] S. Kim, K. Park, C. Choi, M.Y. Ha, D. Lee, Removal of ultrafine particles in a full-scale two-stage electrostatic precipitator employing a carbon-brush ionizer for residential use, Build. Environ. 223 (2022) 109493.
[17] Y. Shi, M. Fang, Q. Wang, K. Yan, J. Cen, Z. Luo, Enhanced high-temperature particle capture through an electrostatic precipitator with assistant electrodes, Sep. Purif. Technol. 324 (2023) 124550.
[18] O. Molchanov, K. Krpec, J. Horák, L. Kuboňová, F. Hopan, Comparison of methods for evaluating particle charges in the electrostatic precipitation of fly-ash from small-scale solid fuel combustion, Sep. Purif. Technol. 248 (2020) 117057.
[19] Q.-Z. Xue, T.-Y. Wen, Separating Al_2O_3 particles from high-speed flue gas by an induced flow recirculation in two-stage electrostatic precipitator, Sep. Purif. Technol. 234 (2020) 116105.
[20] Z. Yang, Y. Tong, L. Zhang, S. Bu, H. Huang, G. Huo, J. Fang, H. Ding, W. Xu, Enhancing fine particle separation by hybrid-electrostatic-turbulence coagulation: an experimental and numerical investigation, Adv. Powder Technol. 33 (2022) 103431.
[21] H. Zhang, L. Shao, W. Gao, Y. Wang, X. Liu, Y. Yang, C. Zheng, X. Gao, Particle charging in electric field under simulated SO_3-containing flue gas at low temperature, Fuel 310 (2022) 122291.
[22] M. Jędrusik, A. Świerczok, A. Jaworek, Collection of low resistivity fly ash in an electrostatic precipitator, J. Phys. Conf. Ser. 418 (2013) 012069.
[23] M. Jędrusik, A. Świerczok, The correlation between corona current distribution and collection of fine particles in a laboratory-scale electrostatic precipitator, J. Electrostat. 71 (2013) 199–203.
[24] M. Jędrusik, A. Świerczok, The influence of unburned carbon particles on electrostatic precipitator collection efficiency, J. Phys. Conf. Ser. 301 (2011) 012009.
[25] M. Rezinkina, O. Rezinkin, F. D'Alessandro, A. Danyliuk, A. Guchenko, S. Lytvynenko, Experimental and modelling study of the dependence of corona discharge on electrode geometry and ambient electric field, J. Electrostat. 87 (2017) 79–85.
[26] R.G.S.A. Andrade, V.G. Guerra, Discharge electrode influence on electrostatic precipitation of nanoparticles, Powder Technol. 379 (2021) 417–427.
[27] X. Wang, J. Chang, C. Xu, P. Wang, L. Cui, C. Ma, Electrical characteristics of electrostatic precipitator with a wet membrane-based collecting electrode, J. Electrostat. 80 (2016) 85–94.
[28] C. Lübbert, U. Riebel, Corona Quenching – Elektroabscheider bei hohen Aerosolkonzentrationen, Chem. Ing. Tech. 83 (2011) 525–534.
[29] U. Riebel, R. Radtke, R. Loos, An experimental investigation on corona quenching, J. Electrostat. 54 (2002) 159–165.
[30] W. Deutsch, Über die Dichteverteilung unipolarer Ionenströme, Ann. Phys. (berlin) 408 (1933) 588–612.
[31] W.T. Sproull, Corona Quenching— *Its* Significance *in* Electrical Precipitation, J. Air Pollut. Control Assoc. 13 (1963) 617–621.
[32] A.A. Elmoursi, G.S.P. Castle, The analysis of corona quenching in cylindrical precipitators using charge simulation, IEEE Trans. Ind. Appl. IA-22 (1986) 80–85.
[33] M.B. Awad, G.S.P. Castle, The efficiency of electrostatic precipitators under conditions of corona quenching, J. Air Pollut. Control Assoc. 25 (1975) 172–176.
[34] Z. Yang, P. Ji, Q. Li, Y. Jiang, C. Zheng, Y. Wang, X. Gao, R. Lin, Comprehensive understanding of SO_3 effects on synergies among air pollution control devices in ultra-low emission power plants burning high-sulfur coal, J. Clean. Prod. 239 (2019) 118096.
[35] J. Podliński, A. Niewulis, A. Berendt, J. Mizeraczyk, Pumping effect measured by PIV method in a multilayer spike electrode EHD device for air cleaning, IEEE Trans. Ind. Appl. 49 (2013) 2402–2408.
[36] J. Podliński, Electrohydrodynamic flow evolution in a narrow wire-plate electrostatic precipitator, Przegląd Elektrotechniczny 2 (2017) 214–218.
[37] J. Podlinski, A. Niewulis, V. Shapoval, J. Mizeraczyk, Electrohydrodynamic secondary flow and particle collection efficiency in a one-sided spike-plate type electrostatic precipitator, IEEE Trans. Dielectr. Electr. Insul. 18 (2011) 1401–1407.
[38] J. Podliński, A. Niewulis, J. Mizeraczyk, Electrohydrodynamic flow and particle collection efficiency of a spike-plate type electrostatic precipitator, J. Electrostat. 67 (2009) 99–104.
[39] J. Mizeraczyk, A. Berendt, J. Podlinski, Temporal and spatial evolution of EHD particle flow onset in air in a needle-to-plate negative DC corona discharge, J. Phys. D Appl. Phys. 49 (2016) 205203.
[40] A. Krupa, J. Podliński, J. Mizeraczyk, A. Jaworek, Velocity field of EHD flow during back corona discharge in electrostatic precipitator, Powder Technol. 344 (2019) 475–486.
[41] E. Moreau, P. Audier, N. Benard, Ionic wind produced by positive and negative corona discharges in air, J. Electrostat. 93 (2018) 85–96.
[42] K. Luo, Y. Li, C. Zheng, X. Gao, J. Fan, Numerical simulation of temperature effect on particles behavior via electrostatic precipitators, Appl. Therm. Eng. 88 (2015) 127–139.
[43] Y. Zhu, M. Gao, M. Chen, J. Shi, W. Shangguan, Numerical simulation of capture process of fine particles in electrostatic precipitators under consideration of electrohydrodynamics flow, Powder Technol. 354 (2019) 653–675.
[44] Y. Song, Y. Zhang, W. Zhu, Y. Liu, W. Long, K. Vafai, Study on the influence of electrodes on the collection efficiency during the treatment of welding fume in electrostatic precipitators, J. Electrostat. 123 (2023) 103808.
[45] M. Hu, X. Wang, Y. Lei, X. Gao, Study on energy saving and emission reduction of high voltage power supply control of ESP, in: 2011 International Conference on Remote Sensing, Environment and Transportation Engineering, 2011: pp. 8538–8541.
[46] A.T. Sobczyk, A. Marchewicz, A. Krupa, A. Jaworek, T. Czech, Ł. Śliwiński, D. Kluk, A. Ottawa, A. Charchalis, Enhancement of collection efficiency for fly ash particles (PM2.5) by unipolar agglomerator in two-stage electrostatic precipitator, Sep. Purif. Technol. 187 (2017) 91–101.
[47] A. Marchewicz, A.T. Sobczyk, A. Krupa, Ł. Śliwiński, A. Jaworek, Particle penetration through industrial scale electrostatic agglomerator, J. Electrostat. 115 (2022) 103670.
[48] A.T. Sobczyk, A. Marchewicz, A. Krupa, Ł. Śliwiński, G. Boryczko, A. Jaworek, Effect of Electrostatic Precipitation and Agglomeration of Particles on Bag Filter Regeneration, in: B. Németh (Ed.), Proceedings of the 16th International Conference on Electrostatic Precipitation, Springer International Publishing, Cham, 2023: pp. 73–89.
[49] L. Zhou, Y. Liu, L. Luo, Z. Yuan, L. Yang, H. Wu, Improving the removal of fine particles by chemical agglomeration during the limestone-gypsum wet flue gas desulfurization process, J. Environ. Sci. 80 (2019) 35–44.

[50] J. Yan, L. Chen, L. Yang, Combined effect of acoustic agglomeration and vapor condensation on fine particles removal, Chem. Eng. J. 290 (2016) 319–327.
[51] H.Y. Choi, Y.G. Park, M.Y. Ha, Numerical simulation of the wavy collecting plate effects on the performance of an electrostatic precipitator, Powder Technol. 382 (2021) 232–243.
[52] M.B. Fayyad, A. Asipuela, T. Iváncsy, The effect of the corona wire distribution with W-type of collecting plates on the characteristics of electrostatic precipitators, J. Electrostat. 125 (2023) 103841.
[53] Y. Tong, L. Liu, L. Zhang, S. Bu, F. Chen, W. Shao, C. Feng, W. Xu, S. Qi, L. Fu, Separation of fine particulates using a honeycomb tube electrostatic precipitator equipped with arista electrodes, Sep. Purif. Technol. 236 (2020) 116299.
[54] Y. Tong, L. Zhang, S. Bu, F. Chen, W. Xu, R. Wu, L. Liu, Y. Xu, Multifield modeling of particle dynamics in an electrostatic precipitator equipped with pointed-end arista on corona, Powder Technol. 362 (2020) 680–689.
[55] A. Niewulis, J. Podlinski, V. Shapoval, J. Mizeraczyk, Collection efficiency in narrow electrostatic precipitators with a longitudinal or transverse wire electrode, IEEE Trans. Dielect. Electr. Insul. 18 (2011) 1423–1428.
[56] S. Arif, D.J. Branken, R.C. Everson, H.W.J.P. Neomagus, L.A. le Grange, A. Arif, CFD modeling of particle charging and collection in electrostatic precipitators, J. Electrostat. 84 (2016) 10–22.
[57] A. Järvinen, M. Aitomaa, A. Rostedt, J. Keskinen, J. Yli-Ojanperä, Calibration of the new electrical low pressure impactor (ELPI$^+$), J. Aerosol Sci 69 (2014) 150–159.
[58] Z. Yang, C. Zheng, X. Zhang, C. Li, Y. Wang, W. Weng, X. Gao, Sulfuric acid aerosol formation and collection by corona discharge in a wet electrostatic precipitator, Energy Fuels 31 (2017) 8400–8406.
[59] C. Wang, J. Sha, H. Yi, J. Mo, J. Ma, Onset Voltage for Electrospray from Nanopores, in, IEEE Int. Conf. Ind. Tech. (ICIT) 2022 (2022) 1–6.